Molecular Cancer Research

Periprostatic Adipose Tissue Favors Prostate Cancer Cell Invasion in an Obesity-Dependent Manner: Role of Oxidative Stress

Victor Laurent[1], Aurélie Toulet[1], Camille Attané[1], Delphine Milhas[1], Stéphanie Dauvillier[1], Falek Zaidi[2], Emily Clement[1], Mathieu Cinato[3], Sophie Le Gonidec[3], Adrien Guérard[1], Camille Lehuédé[1], David Garandeau[1], Laurence Nieto[1], Edith Renaud-Gabardos[3], Anne-Catherine Prats[3], Philippe Valet[3], Bernard Malavaud[4], and Catherine Muller[1]

Abstract

Prostate gland is surrounded by periprostatic adipose tissue (PPAT), which is increasingly believed to play a paracrine role in prostate cancer progression. Our previous work demonstrates that adipocytes promote homing of prostate cancer cells to PPAT and that this effect is upregulated by obesity. Here, we show that once tumor cells have invaded PPAT (mimicked by an *in vitro* model of coculture), they establish a bidirectional crosstalk with adipocytes, which promotes tumor cell invasion. Indeed, tumor cells induce adipocyte lipolysis and the free fatty acids (FFA) released are taken up and stored by tumor cells. Incubation with exogenous lipids also stimulates tumor cell invasion, underlining the importance of lipid transfer in prostate cancer aggressiveness. Transferred FFAs (after coculture or exogenous lipid treatment) stimulate the expression of one isoform of the pro-oxidant enzyme NADPH oxidase, NOX5. NOX5 increases intracellular reactive oxygen species (ROS) that, in turn, activate a HIF1/MMP14 pathway, which is responsible for the increased tumor cell invasion. In obesity, tumor-surrounding adipocytes are more prone to activate the depicted signaling pathway and to induce tumor invasion. Finally, the expression of NOX5 and MMP14 is upregulated at the invasive front of human tumors where cancer cells are in close proximity to adipocytes and this process is amplified in obese patients, underlining the clinical relevance of our results.

Implications: Our work emphasizes the key role of adjacent PPAT in prostate cancer dissemination and proposes new molecular targets for the treatment of obese patients exhibiting aggressive diseases.

Introduction

Malignant evolution of solid cancers relies on complex cell-to-cell interactions sustained by a broad network of physical and chemical mediators that constitute the tumor microenvironment (1). Adipose tissue, and its main cellular component, adipocytes, have recently emerged as key actors in solid tumor progression (2). Upon proximal adipose tissue infiltration, a bidirectional crosstalk takes place between invasive tumor cells and adipocytes. Initially described in breast cancer, tumor-surrounding adipocytes exhibit extensive phenotypical changes defined by a decrease in lipid content, a decreased expression of adipocyte markers, and an activated state demonstrated predominantly by the overexpression of proinflammatory cytokines and ECM (extracellular matrix)-related molecules (3). We named these cells cancer-associated adipocytes (CAA; ref. 3). Occurrence of CAAs is not restricted to breast cancer and has been described in a wide range of solid tumors including metastatic ovarian cancer, renal and colon cancers, as well as melanoma (2). In turn, CAAs promote tumor aggressiveness by secreting soluble factors, ECM proteins, and ECM-remodeling enzymes and by modulating tumor cell metabolism (2). The decrease in size and lipid content of tumor-surrounding adipocytes results from a "dedifferentiation" process depending on the reactivation of the Wnt/β-catenin pathway in response to Wnt3a secreted by tumor cells (4) and from induction of lipolysis, the latter process resulting in release of free fatty acids (FFA; refs. 5–7). These FFAs are then taken up, stored in lipid droplets, and used by tumor cells, where they have been described to contribute to tumor progression mainly through modulation of tumor cell metabolism toward fatty acid oxidation (FAO; refs. 5–7). This metabolic symbiosis instilled between cancer cells and tumor-surrounding adipocytes is only beginning to be explored but could provide new therapeutic targets as we recently reviewed in ref. 8. In addition to FAO, FFAs acquired from adipocytes could be used as membrane building blocks and/or signaling lipids and the fate of these lipids may depend on the tumor cell type.

Among the different types of tumors whose close interaction with adipose tissue could influence tumor progression is prostate cancer, the most common malignancy in men in Western

[1]Institut de Pharmacologie et de Biologie Structurale (IPBS), Université de Toulouse, CNRS, UPS, Toulouse, France. [2]Service d'Anatomo-Pathologie, Institut Universitaire du Cancer, Toulouse, France. [3]Institut des Maladies Métaboliques et Cardiovasculaires (I2MC), Université de Toulouse, Inserm UMR 1048, UPS, Toulouse, France. [4]Département d'Urologie, Institut Universitaire du Cancer, Toulouse, France.

Note: Supplementary data for this article are available at Molecular Cancer Research Online (http://mcr.aacrjournals.org/).

V. Laurent and A. Toulet contributed equally to this article.

C. Attané and D. Milhas contributed equally to this article.

Corresponding Author: Catherine Muller, IPBS CNRS UMR 5089, 205 Route de Narbonne, Toulouse 31077, France. Phone: 335-6117-5932; Fax: 335-6117-5933; E-mail: muller@ipbs.fr

doi: 10.1158/1541-7786.MCR-18-0748

countries. The prostate is surrounded by periprostatic adipose tissue (PPAT) and extraprostatic extension into PPAT is a widely acknowledged adverse prognostic factor in prostate cancer and an important determinant of prostate cancer recurrence after treatment (9). The positive association between obesity and aggressive prostate cancer, defined by an increase in local and distant dissemination, is also in favor of a role for adipose tissue in tumor progression (10). We have recently demonstrated that adipocytes from PPAT favor the initial step of PPAT infiltration by secreting the CCL7 chemokine that attracts CCR3-expressing cancer cells, and this process is amplified in obesity (11). Prostate-confined cancer cell migration and invasion may also be promoted at distance by inflammatory cytokines and metalloproteases secreted by PPAT, as well as by adipocyte-derived exosomes (12–14). In contrast to other cancer types such as breast or ovarian cancer (2), the effect of the invaded cancer cells on adipocytes within PPAT has been poorly described. Secretions from PPAT are modified by tumor-conditioned medium with upregulation of osteopontin, TNFα, and IL6, highlighting that, like other adipose depots, it is not inert to tumors (15). Coculture of prostate cancer cells with rat epididymal adipocytes increases growth and changes the morphology of prostate cancer cells (16, 17), but phenotypical changes of adipocytes have not been investigated in these studies. In addition, the mechanisms that govern increased prostate cancer cell aggressiveness in the presence of adipocytes are poorly described and have been mainly attributed to soluble factors (such as IL6; for review, see ref. 18). Finally, lipid transfer has not been demonstrated between periprostatic adipocytes and tumor cells, but only with bone marrow–derived adipocytes present at prostate cancer's most frequent metastatic site (19, 20). Here, we demonstrate that prostate cancer cells are able to induce a CAA phenotype *in vitro* and *in vivo*, and that CAAs, in turn, promote tumor invasion. Lipid transfer between tumor-surrounding adipocytes and cancer cells promotes tumor aggressiveness by inducing oxidative stress in a NADPH oxidase–dependent manner, activating a proinvasive signaling pathway. The overall pathway is amplified in obesity and has been validated in human tumors. This study highlights the importance of lipid transfer in the tumor-promoting effect of adipocytes but also underlines that the consequence of this process is not univocal among all tumor types.

Materials and Methods

Antibodies

Polyclonal antibodies against matrix metalloproteinase-2 and 9 (MMP2 and MMP9) were from Chemicon International Inc and used for Western blot experiments. The polyclonal antibody against MMP14 was from Santa Cruz Biotechnology and was used for Western blot and IHC. The mAb against HIF1α (clone H1α67) and the polyclonal antibody against NOX5 were from Novus Biologicals and were used, respectively, for Western blot and IHC. The mAb against HIF1β (clone H1β234) was from Novus Biologicals and was used for Western blot experiments. The mAb against carbonic anhydrase IX (CAIX) and the polyclonal antibody against GLUT1 were, respectively, from BioScience Slovakia and from Spring Bioscience and were used for Western blot experiments. The mAb against α-tubulin (clone Ab-2) was from Thermo Fisher Scientific and was used for Western blot experiments.

Probes and chemical reagents

The inhibitor targeting NADPH oxidases, diphenyliodonium (DPI; used at 10 μmol/L), NAC (used at 10 mmol/L), complex I or III of respiratory chain inhibitors [antimycin A (used at 10 μmol/L) and rotenone (used at 5 μmol/L), respectively] were obtained from Sigma-Aldrich. The Bodipy 493/503 lipid probe (used at 1 μg/mL), DAPI (used at 1 μmol/L) and the carboxy-H_2DCFDA ROS probe (used at 10 μmol/L) were obtained from Life Technologies. Palmitate (used at 100 μmol/L), intralipids 20% emulsion (used at 0.01%), and hydrogen peroxide solution (30% w/w; used at 5 μmol/L) were purchased from Sigma-Aldrich.

Cell culture

The human prostate tumor cell lines C4-2B (from DSMZ), Du-145 (ATCCHTB-81), and PC-3 (ATCCCRL-1435; provided by Dr Olivier Cuvillier, IPBS, Toulouse, France) were used in this study. Cells were cultured in RPMI medium (Invitrogen) supplemented with 10% FCS, 125 mg/mL streptomycin, 125 IU/mL penicillin. All cell lines used in this study were grown in a humid atmosphere with 5% CO_2 at 37°C. All the cell lines were used within 2 months after thawing of frozen aliquots. Cell lines were authenticated on the basis of viability, recovery, growth, and morphology. The murine 3T3-F442A preadipocyte cell line was grown and differentiated into mature adipocytes as described previously (21). The term "adipocyte" refers to cells that have been differentiated for 10 to 14 days. The differentiation phenotype of mature adipocytes was routinely assessed by Red Oil staining as described previously (21). Tumor cell conditioned medium (CM) was obtained by incubating the cells in RPMI medium containing no FCS and 1% BSA (Sigma-Aldrich), for 12 hours after which the medium was harvested and immediately stored at −80°C. Aliquots were used only once.

Coculture system

Cocultures between tumor cells and adipocytes were performed using a Transwell culture system with 0.4-μm pores (Millipore). A total of 7×10^4 (PC-3 and Du-145) or 1.5×10^5 (C4-2B) cells were seeded in the top chamber of the Transwell system in supplemented DMEM (Invitrogen) and cocultivated or not with mature adipocytes (grown either in 2D for 3T3-F442A mature adipocytes or in 3D for primary isolated adipocytes, detailed below) for 3 days. Adipocytes or tumor cells cultivated alone in the system served as controls.

siRNA transfection

Transient transfection of prostate tumor cells (PC-3) was performed using the Dharmafect1 transfection reagent according to the manufacturer's specifications. Briefly, 2×10^4 cells were seeded in an insert and incubated for 12 hours at 37 °C. Then, cells were mixed with 500 nmol/L of either control nontargeting siRNA (siCtrl; ON-TARGETplus non-targeting Pool D-001810–10), human MMP14 siRNA1 (si1MMP14; ON-TARGETplus J-004145-13), MMP14 siRNA2 (si2MMP14; ON-TARGETplus J-004145-14), or a pool of human HIF1α siRNA (ON-TARGET plus SMARTpool J-004018-07) synthesized by Dharmacon (Dharmacon, Inc.). Twenty-four hours after transfection, medium containing transfection reagent was replaced by normal culture medium.

Table 1. List of primers

Genes	Species	Primer forward	Primer reverse	[C]
NOX2	Hu	5′GCCCAAAGGTGTCCAAGCT	5′TCCCCAAGCATGCGGATAT	500 nmol/L
NOX5	Hu	5′TGTTGATCCAGATAAAGTCCACCTT	5′CAGGCACCAGAAAAGAAAGCAT	500 nmol/L
GAPDH	Hu/Mu	5′TGCACCACCAACTGCTTAGC	5′GGATGGACTGTGGTCATGAG	500 nmol/L
HPRT	Hu	5′TGACACTGGCAAAACAATGCA	5′GCTTGCGACCTGACCATCT	500 nmol/L
Lipe	Mu	5′GGCTTACTGGGCACAGATACCT	5′CTGAAGGCTCTGAGTTGCTCAA	900 nmol/L
Adipoq	Mu	5′TGGAATGACAGGAGCTGAAGG	5′TATAAGCGGCTTCTCCAGGCT	900 nmol/L
Retn	Mu	5′TCGTGGGACATTCGTGAAGA	5′GGGCTGCTGTCCAGTCTATCC	300 nmol/L
Fabp4	Mu	5′TTCGATGAAATCACCGCAGA	5′GGTCGACTTTCCATCCCACTT	900 nmol/L
Cebpa	Mu	5′CAAGAACAGCAACGAGTACCG	5′GTCACTGGTCAACTCCAGCAC	100 nmol/L
Mmp11	Mu	5′GCCCTCATGTCCCCTTTCTAC	5′CCTTCGGTCATCTGGGCTAA	900 nmol/L
Pai1	Mu	5′TCTCCAATTACTGGGTGAGTCAGA	5′GCAGCCGGAAATGACACAT	900 nmol/L
Hprt	Mu	5′TGGCCATCTGCCTAGTAAAGC	5′GGACGCAGCAACTGACATTTC	500 nmol/L

Mice, isolation of murine primary adipocytes, and 3D culture

C57BL/6J male mice obtained from Janvier (Le Genest-Saint-Isle, France) were handled in accordance with the National Institute of Medical Research's (INSERM) principles and guidelines. The protocols used for feeding the mice either with normal or high-fat diet (abbreviated ND and HFD, respectively) as well as the isolation of perigonadal adipocytes have been described previously (11). Adipocytes were then embedded in a 3D collagen gel matrix. To prepare the collagen gel culture system, type I collagen was diluted to 2 mg/mL (Nitta Gelatin Co Ltd) in DMEM, 10% FCS, and 0.75% sodium bicarbonate. Primary adipocytes were gently mixed with this solution before adding 6×10^5 adipocytes to 6-well plates. The culture dish was immediately placed at 37°C to allow the gel to form, which was then covered with DMEM containing 10% FCS and 50 nmol/L insulin. Then, the top layer of the Transwell system containing prostate cancer cells was added to the 6-well plates for coculture experiments during 3 days.

Metastasis assay

These experiments were performed as described previously (3). Briefly, a total of 1×10^6 PC-3 cells, previously cocultivated or not with mature adipocytes for 3 days, in the presence or not of DPI (10 μmol/L), were injected intravenously in nude mice (5 animals per condition). Mice were sacrificed 25 days later and lungs were immediately excised for analysis. For this, lungs were fixed in 4% paraformaldehyde and embedded in paraffin. Sections were stained with hematoxylin and eosin (H&E) and the number of micrometastases per slice was counted. The local Institutional Animal Care and Use Committee approved the experimental protocols described in the study.

Human periprostatic adipose tissue samples

Human periprostatic adipose tissue samples (HuPPAT) samples were collected from radical prostatectomy in accordance with the recommendations of the ethics committee of the Rangueil Hospital (Toulouse, France). All patients gave their informed consent to participate to this study, which was conducted in accordance with the Declaration of Helsinki as revised in 2000. Periprostatic adipose tissue samples were collected at distance from the tumors, and were macroscopically devoid of fibrosis as described previously (11). These samples were collected and treated within 15 minutes after the surgery thus ensuring the preservation of labile molecules. Primary adipocytes were isolated and embedded in a three-dimensional collagen gel matrix as described above. For each experiment, three independent patient samples were used from nonobese individuals (20 kg/m^2 < BMI < 30 kg/m^2).

Boyden chamber invasion assays

After 3 days of coculture with 3T3-F442A adipocytes or primary adipocytes, prostate tumor cells were trypsinized and submitted to Matrigel invasion assays as described previously (7, 22). When indicated, cells were preincubated for 30 minutes at 37°C with the indicated inhibitors.

RNA extraction and quantitative PCR

RNA extraction, reverse transcription, and quantitative PCR (qPCR) were conducted as described previously (11). All the primers used in this study are presented in Table 1.

Western blot analysis

Whole-cell extracts and immunoblots were performed as described previously (23).

Intracellular ROS measurement

Intracellular ROS were determined by flow cytometry using H2-DCFDA (Life Technologies) as a fluorescent probe. Briefly, cells were incubated with 10 μmol/L H2-DCFDA for 30 minutes at 37°C, after which they were washed, resuspended in PBS, and immediately analyzed for fluorescence intensity by FACScan flow cytometer (Beckton Dickinson) using a 488 nm excitation beam and a 538 nm band-pass filter. Mean fluorescence intensity was quantified by CellQuest software (Becton Dickinson). When inhibitors were used, ROS production was detected by nitroblue tetrazolium (NBT) assay in which NBT is reduced by ROS to a dark-blue, insoluble form of NBT called formazan. Briefly, cells were incubated for 90 minutes in PBS containing 0.2% NBT and then formazan was dissolved in 50% acetic acid, and the absorbance was measured at 560 nm.

Measure of adipocyte lipolysis

As described previously (7), glycerol released by adipocytes, incubated or not with CM from the indicated cell lines for 3 days, was measured using the glycerol-free reagent kit (Sigma-Aldrich).

Bodipy staining on 3D culture

Adipocytes embedded in a collagen I matrix were fixed in 3.7% paraformadehyde for 60 minutes, washed and then permeabilized in PBS with 0.1% TritonX-100 for 15 minutes. After blocking with 10% FCS, 2% BSA, and 0.1% TritonX-100 in PBS for 60 minutes, adipocytes were incubated with Bodipy 493/503 (1 μg/mL) to measure lipid accumulation (60 minutes, at room temperature). Adipocytes were examined using an Olympus FV-1000 confocal microscope with a 60× oil PLAPON OSC objective (1.4 N.A.). At least three independent experiments were

performed. Images were processed to filter noise with ImageJ software and a similar filter was used to analyze all acquisitions for the experiment. Adipocyte area was measured with ImageJ software.

Confocal microscopy

Cells were seeded on glass coverslips, fixed, and permeabilized as described previously (7). After blocking with 10% FCS and 2% BSA in PBS for 60 minutes, cells were incubated for 30 minutes with rhodamin-phalloidin (1:200) to stain actin cytoskeleton or with Bodipy 493/503 (1 μg/mL) to stain neutral lipids and for 15 minutes with DAPI (1 μmol/L) to stain nucleus. Coverslips were examined using an Olympus FV-1000 with 60× oil PLAPON OSC objective (1.4 N.A.). A minimum of three independent experiments were performed. Images were processed to filter the noise with ImageJ software and a similar filter was used to analyze all acquisitions for the experiment. For the quantification of lipid accumulation, lipid droplet area per cell was quantified with ImageJ software. The invasive front is defined as areas at the edge of tumors in which tumor cells have begun to invade the surrounding stroma and, notably, are found at close proximity to surrounding adipocytes (up to 200 μm from the tumor mass), as stated in our previous studies (3, 7, 11).

Histology and IHC on prostate tumor tissue

To measure adipocyte area, tumor tissue (from three independent patients) was fixed in 4% paraformaldehyde and embedded in paraffin. Then, sections were stained with hematoxylin and eosin (H&E) and adipocyte area was measured with ImageJ software (a total of 120 adipocytes). Frozen tissues obtained after radical prostatectomy of 20 patients with pT3a or pT3b prostate cancer, defined by two pathologists (Drs. Catherine Mazerolles and Youri Soucrier), were analyzed for MMP14 and NOX5 expression. Lean patients had a mean BMI of 24.1 ± 2 kg/m^2, whereas obese patients had a mean BMI of 30.7 ± 1.8 kg/m^2. All these patients underwent surgery between February 1, 2010 and December 1, 2011 in the Department of Urology of the University Hospital of Toulouse (directed by Pr. Rischmann) and signed a consent form for the use of their tissue samples for scientific purposes before surgical intervention. NOX5 and MMP14 staining was performed and quantified as described previously (11). Intensity for each staining was quantified after manual selection of the area of interest (tumor center or invasive front), under the supervision of pathologists, who were blind to clinical data.

Statistical analysis

The statistical significance of differences between the means was evaluated using unpaired Student *t* tests. All statistical tests were two-sided. *P* values below 0.05 (*), <0.01 (**), <0.001 (***), and <0.0001 (****) were deemed as significant while "NS" stands for not significant.

Results and Discussion

A bidirectional crosstalk is observed between prostate cancer cells and adipocytes *in vitro* and *in vivo*

The crosstalk between prostate cancer cell lines and mature adipocytes was first investigated *in vitro* using a coculture system originally described by our group in breast cancer (3). Three human prostate cancer cell lines (C4-2B, Du-145, and PC-3), exhibiting increased aggressiveness, were grown on Transwells, allowing the diffusion of soluble factors, in the presence or not of mature adipocytes. After 3 days, tumor cells were trypsinized and Matrigel invasion assays were performed. As shown in Fig. 1A, invasion toward serum-containing medium was increased in cells previously cocultivated with adipocytes as compared with tumor cells grown alone. Accordingly, cocultivated tumor cells exhibited a more scattered aspect and developed multiple extended protrusions as shown by actin staining (Fig. 1B), suggesting that an epithelial–mesenchymal transition takes place, as already demonstrated in many cancer cell models cocultivated with adipocytes (2). This proinvasive effect was not observed when tumor cells were cocultivated with preadipocytes (Supplementary Fig. S1A). In addition, the proinvasive effect was dissociated from a tumor growth–promoting effect, as no increase in cell number was observed in cocultivated, as compared with control cells (Supplementary Fig. S1B). We then investigated the phenotypic changes induced by coculture in mature adipocytes. According to our previous results using breast cancer cell lines and tumors (3), cocultivated adipocytes exhibited a CAA phenotype (Fig. 1C). We observed a strong decrease in mRNA levels of several terminal differentiation markers such as hormone-sensitive lipase (*Lipe*), adiponectin (*Adipoq*), resistin (*Retn*), fatty acid binding protein 4 (*Fabp4*), and CCAAT/enhancer-binding protein alpha (*Cebpa*) in cocultivated adipocytes when compared with control cells (Fig. 1C, left). This was associated with an activated state characterized by overexpression of *Mmp11* and plasminogen activator inhibitor-1 (*Pai1*; Fig. 1C, right). A dramatic decrease in the number and size of lipid droplets was observed in mature adipocytes cocultivated with PC-3 cells as revealed by neutral lipid staining (Bodipy 493/503; Fig. 1D). Conversely, cocultivated PC-3 displayed an increase in small lipid droplets (Fig. 1D). The breakdown of triglycerides stored in fat cells through lipolysis leads to release of glycerol and FFAs (Fig. 1E, top). Accordingly, CM from different prostate cancer cell lines increases adipocyte lipolysis as revealed by a rise in glycerol release after incubation with adipocytes (Fig. 1E, bottom). Catecholamines are considered as major regulators of lipolysis. β-adrenergic receptor (AR) activation elicits a G protein–coupled cascade leading ultimately to the phosphorylation and activation of HSL (24). Contrarily, by binding to α2-AR, catecholamines could also exert a major antilipolytic effect, which is abrogated in the presence of α2-AR antagonists (24). As shown in Supplementary Fig. S2, we found that neither propranolol (β-AR antagonist) nor UK14304 (α2-AR agonist) were able to inhibit the lipolysis induced by tumor secretions, therefore eliminating the role of catecholamines in this process. Remarkably, at the invasive front of human prostate cancers, adipocytes from PPAT exhibited a strong decrease in size and lipid content, highlighting the clinical relevance of our results (Fig. 1F). To our knowledge, this is the first time that the CAAs have been documented in prostate cancer both *in vitro* and in human tumors. This phenomenon, which we originally described, seems to occur at the primary site of all solid tumors that grow in an adipocyte-rich microenvironment (2). At cellular levels, the occurrence of a CAA phenotype is probably a complex process associating both dedifferentiation (Fig. 1C) and induction of lipolysis (Fig. 1E). In breast cancer, we have demonstrated that this dedifferentiation process was due to the reactivation of Wnt/β-catenin pathway, a pathway that was also shown to be involved in pancreatic cancer (25). The signal emanating from tumor cells that is responsible for the lipolytic process remains unknown. In our study (Supplementary Fig. S2), as well as in breast cancer (7),

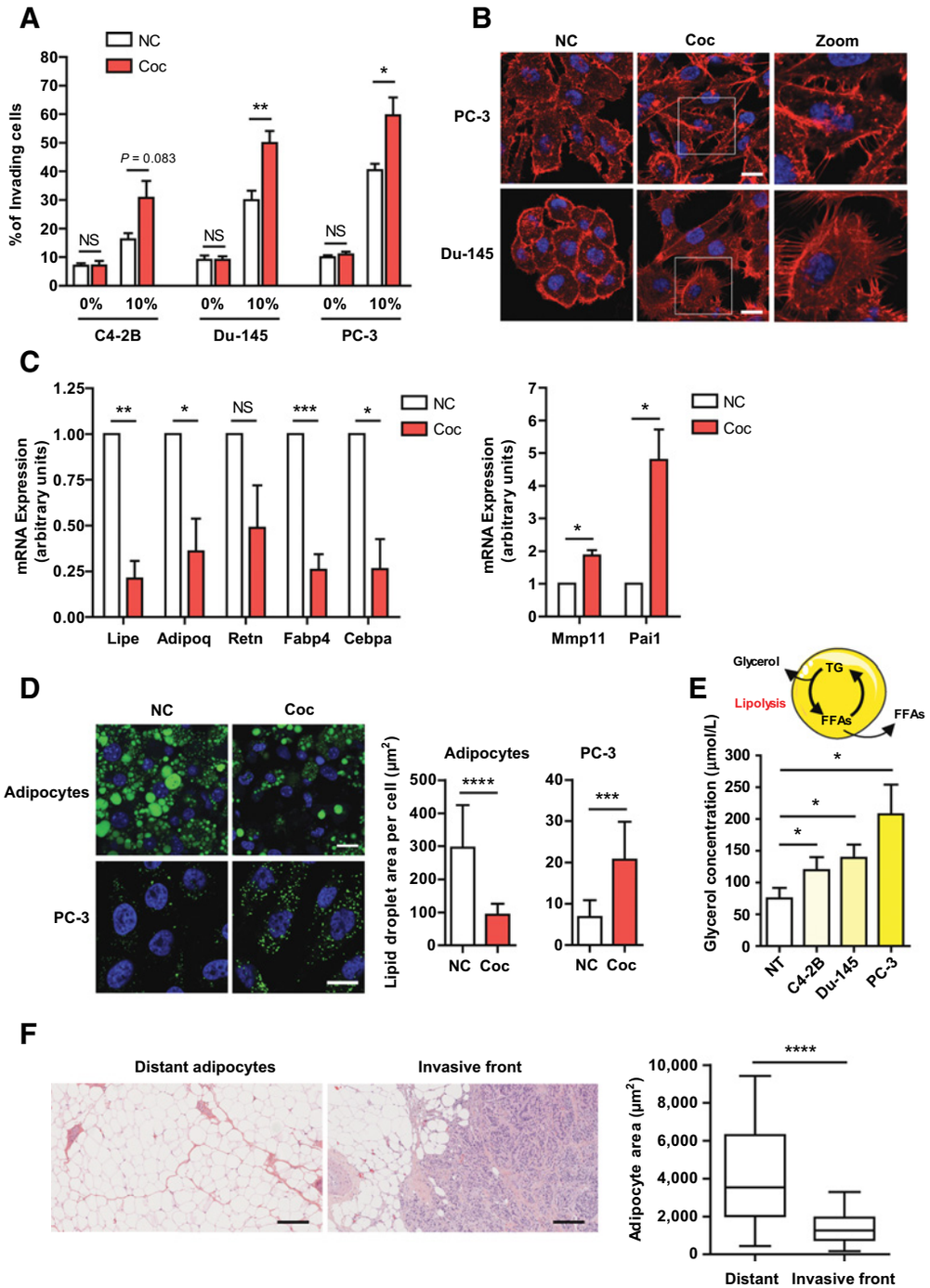

Figure 1.

A bidirectional crosstalk occurs between prostate cancer cells and adipocytes *in vitro* and *in vivo*. **A–D,** Indicated prostate cancer cell lines were cocultivated (Coc) or not (NC) with adipocytes for 3 days. **A,** Matrigel invasion assays towards a medium containing either 0% or 10% FCS were performed in prostate cancer cells. **B,** Actin was labeled with rhodamine-phalloidin (red) and nuclei were labeled with DAPI in prostate cancer cells. Scale bars, 20 µm. The white box indicates a zoomed crop of this area. **C,** After 3 days of coculture with PC3 cells, mRNAs were extracted from adipocytes and expression of the indicated genes was analyzed by qRT-PCR. **D,** Left, lipid droplets were labeled with Bodipy 493/503 (green) and nuclei were labeled with DAPI in mature adipocytes and PC-3 cells. Scale bars, 20 µm. Right, quantification of lipid droplet area performed with ImageJ software. **E,** Graphic representation of the lipolytic process occurring in adipocytes (top). Glycerol release was detected in mature adipocytes treated or not (NT) with prostate cancer cell CM (C4–2B, Du-145, PC-3) for 3 days (bottom; $n = 4$). **F,** Left, H&E staining of adipocytes (white cells) distant from the tumor or at the invasive front of prostate cancer (original magnification, × 20). Scale bars, 200 µm. Right, quantification of mean adipocyte area at the invasive front or in adipose tissue distant from the tumors performed in five independent invasive prostate tumors. Bars and error bars represent the means ± SEM of independent experiments ($n = 3$, unless specified otherwise). Statistically significant by Student *t* test (*, $P < 0.05$; **, $P < 0.01$; ***, $P < 0.001$; ****, $P < 0.0001$; and NS, not significant).

lipolysis is induced through a nonadrenergic pathway that could potentially involve a wide range of biomolecules (24, 26). However, further studies are required to determine the specific actors involved.

Coculture of prostate cancer cells with adipocytes increases oxidative stress in a NADPH oxidase–dependent manner leading to increased invasion

It was generally thought that cancer cells rely mostly on *de novo* lipogenesis rather than exogenous FFAs for generation of intracellular lipids, especially in prostate cancer in which fatty acid synthase (FAS) expression is increased during tumor transformation and progression (27). We show here that prostate cancer can incorporate FFAs from neighboring adipocytes, and similar uptake of exogenous lipids (palmitate) has been shown to occur in several prostate cancer models (28). As shown in Fig. 2, exposure of prostate cancer cells to exogenous saturated or unsaturated FFAs for 3 days also recapitulated the invasive phenotype observed after coculture (Fig. 2A), associated with lipid droplet accumulation and actin reorganization toward a more scattered phenotype (Fig. 2B). As described in the introduction, the transferred FFAs from adipocytes have been previously shown to stimulate tumor aggressiveness through increased FAO in ovarian and breast cancers (5, 7). In breast cancer, the increased tumor invasion induced by coculture with adipocytes was completely abrogated by inhibition of FAO, which was not coupled with ATP production and, in fact, was associated with a decrease in the oxygen consumption rate (OCR; ref. 7). The effect was related to the overexpression of IF1 (inhibitory factor 1, IF1) in cocultivated cells, which specifically inhibits F0F1-ATP synthase (7). As shown in Supplementary Fig. S3, a similar metabolic remodeling occurs in prostate cancer cells. Cocultivated cells exhibited an increase in FAO activity, as compared with control cells, which was efficiently decreased by etomoxir, a drug that inhibits the entry of FFAs into mitochondria by blocking the activity of the long-chain FA transporter, carnitine palmitoyl transferase 1 (CPT1; Supplementary Fig. S3A). In contrast, no increase in basal or coupled OCR was observed in cocultivated cells showing that FAO was not coupled to ATP production (Supplementary Fig. S3B). In addition, lactate production was increased by 2-fold upon coculture (Supplementary Fig. S3C), suggesting that a glycolytic switch has occurred in these cells. However, in contrast to our previous results in breast cancer cells (7), etomoxir had no effect on prostate cancer cell invasion in response to coculture (Supplementary Fig. S3D), suggesting that the increased FAO is not key to the increase in prostate cancer aggressiveness. Recently, Huang and colleagues showed that osteopontin enhances invasion in a CPT1-dependant manner in prostate cancer cells cocultivated with adipose tissue from obese transgenic mice (specific loss of p62 in adipocytes; ref. 29). Importantly, the adipose tissue used in the indicated study is highly infiltrated by macrophages which secrete osteopontin, suggesting that these cells are responsible for the observed increase in tumor cell invasion in this model (29). Thus, different AT components (e.g., adipocytes and macrophages) increase prostate cancer cell invasion through different mechanisms. One of the hallmarks of prostate cancer is increased ROS production, which is linked to a highly invasive and metastatic phenotype (30). In accordance with previously published data (31), we found that intracellular ROS levels rise progressively in prostate cancer cell lines with increasing levels of aggressiveness, as defined by their invasiveness (ref. 11; Supplementary Fig. S4A). Treatment of prostate cancer cells with exogenous ROS such as hydrogen peroxide (H_2O_2) leads to an increased cell invasion in a dose-dependent manner (Supplementary Fig. S4B). As shown in Fig. 2C, PC-3 cells exhibited an increase in intracellular ROS content after 3 days of coculture with mature adipocytes or after treatment with exogenous FFAs but not when cocultivated with preadipocytes. Treatment with the ROS scavenger called NAC (at a dose that is without effect on cell survival, see Supplementary Fig. S5A) abolished the intracellular ROS increase (Fig. 2D) and cell invasion (Fig. 2E) induced by both coculture and treatment with FFAs. In epithelial tumor cells, ROS can derive from various mechanisms including increased metabolism associated with dysfunctional mitochondria (involving the complexes I and III of respiratory chain) or abnormal expression of NADPH oxidases (NOX) enzymes (ref. 32; Fig. 3A). To identify the source of ROS generation induced by lipid uptake, a set of molecules was used that inhibit mitochondrial complex I (rotenone) or complex III (antimycin A) or NOXs (diphenyliodonium, DPI; Fig. 3A). DPI selectively inhibited ROS generation induced by coculture and exogenous lipids, whereas rotenone and antimycin A had no significant effect (Fig. 3B). Similar response patterns were observed when cell invasion was considered (Fig. 3C). Note that, in these experimental conditions, after 3 days of treatment, the dose of DPI used (10 μmol/L) only slightly decreased cell number (Supplementary Fig. S5B). We obtained similar results with another prostate cancer cell line, Du-145 (Supplementary Fig. S6). The absence of involvement of mitochondrial ROS production is in accordance with our previous results showing that OCR is not increased in cocultivated cells (Supplementary Fig. S3B). In line with our results, it has been shown that prostate cancer cells rely mostly on extramitochondrial ROS production to generate oxidative stress (31), and we show here that this process is enhanced upon coculture or treatment with exogenous lipids. DPI is a broad inhibitor of NOXs, a family that contains 7 isoforms (33). In these prostate cancer cell lines, only *NOX2* and *NOX5* are expressed but only *NOX5* expression was upregulated (by about 4-fold) in cocultivated, when compared with noncocultivated tumor cells. Similar results were observed when tumor cells were treated with palmitate, although the increase in *NOX5* expression was less pronounced (Fig. 3D). This could be explained by the contribution of other FFA species, different concentrations of palmitate or additional soluble signals emanating from adipocytes. In our study, we were unable to use a *NOX5* gene-silencing approach as PC-3 cells stably expressing different short hairpin RNAs against NOX5 died within 1 to 2 weeks after transduction. To note, cells transfected with shCtrl grew similarly to nontransfected cells (data not shown). Effects of NOX5 depletion on prostate cancer growth and survival have also been described in previous studies (34, 35). Similar results were obtained with transient transfection with shNOX5, where a clear decrease in cell number was observed 48 hours after transfection (Supplementary Fig. S7). Thus, according to these results, and due to the fact that only *NOX5* was upregulated in our conditions, DPI was chosen as an adapted NOX5 inhibition strategy. To validate whether adipocyte-induced oxidative stress is involved in prostate cancer invasion *in vivo*, PC-3 cells cocultivated with adipocytes for 3 days and treated or not with DPI, were injected intravenously into nude host mice. As shown in Fig. 3E, the number of lung metastases was enhanced in mice injected with PC-3 cells previously cocultivated with adipocytes as compared with mice injected with PC-3 grown alone. The

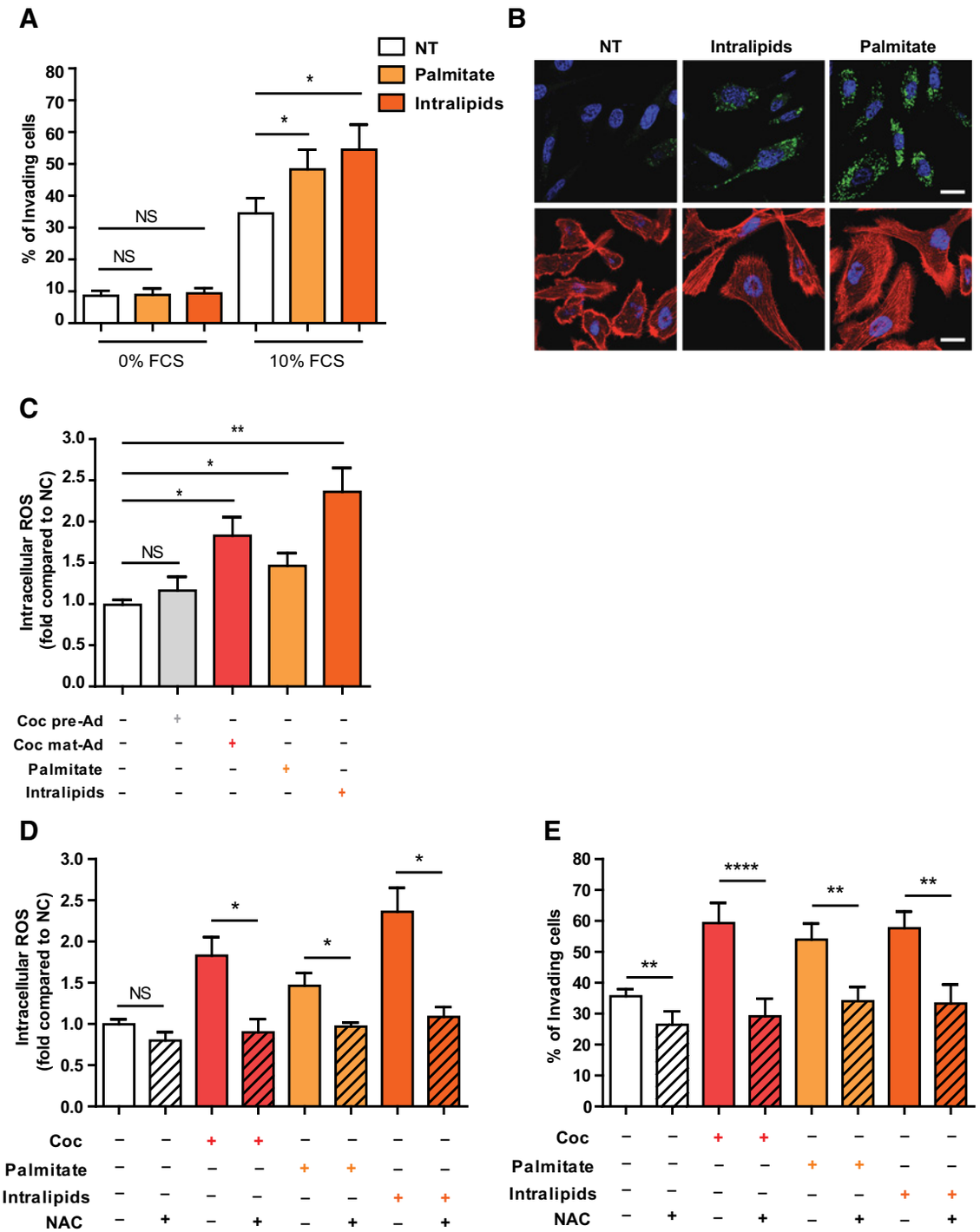

Figure 2.

Coculture induces an increase in prostate cancer intracellular ROS level that is reproduced by exogenous lipids. **A** and **B,** PC-3 cells were treated or not (NT) with 0.01% intralipids or 100 μmol/L palmitate for 3 days. **A,** Matrigel invasion assays were performed toward a medium containing 0% or 10% FCS. **B,** Cells were stained with Bodipy 493/503 (top) or rhodamine-phalloidin (bottom) and nuclei were labeled with DAPI. Scale bars, 20 μm. **C,** Intracellular ROS accumulation was measured by flow cytometry using H2-DCFDA in PC-3 cocultivated (Coc) or not (NC) with 3T3-F442A preadipocytes (Coc pre-Ad) or with mature adipocytes (Coc mat-Ad) or treated with 0.01% intralipids or 100 μmol/L palmitate. **D,** Intracellular ROS accumulation measured by NBT assay in PC-3 cells cocultivated (Coc) with adipocytes or treated with 0.01% intralipids or 100 μmol/L palmitate in the presence or absence of 10 mmol/L NAC. **E,** Matrigel invasion assays toward a medium containing 10% FCS in PC-3 cells treated in similar conditions. Bars and error bars represent the means ± SEM of independent experiments ($n = 3$). Statistically significant by Student t test (*, $P < 0.05$; **, $P < 0.01$; ****, $P < 0.0001$; NS, not significant).

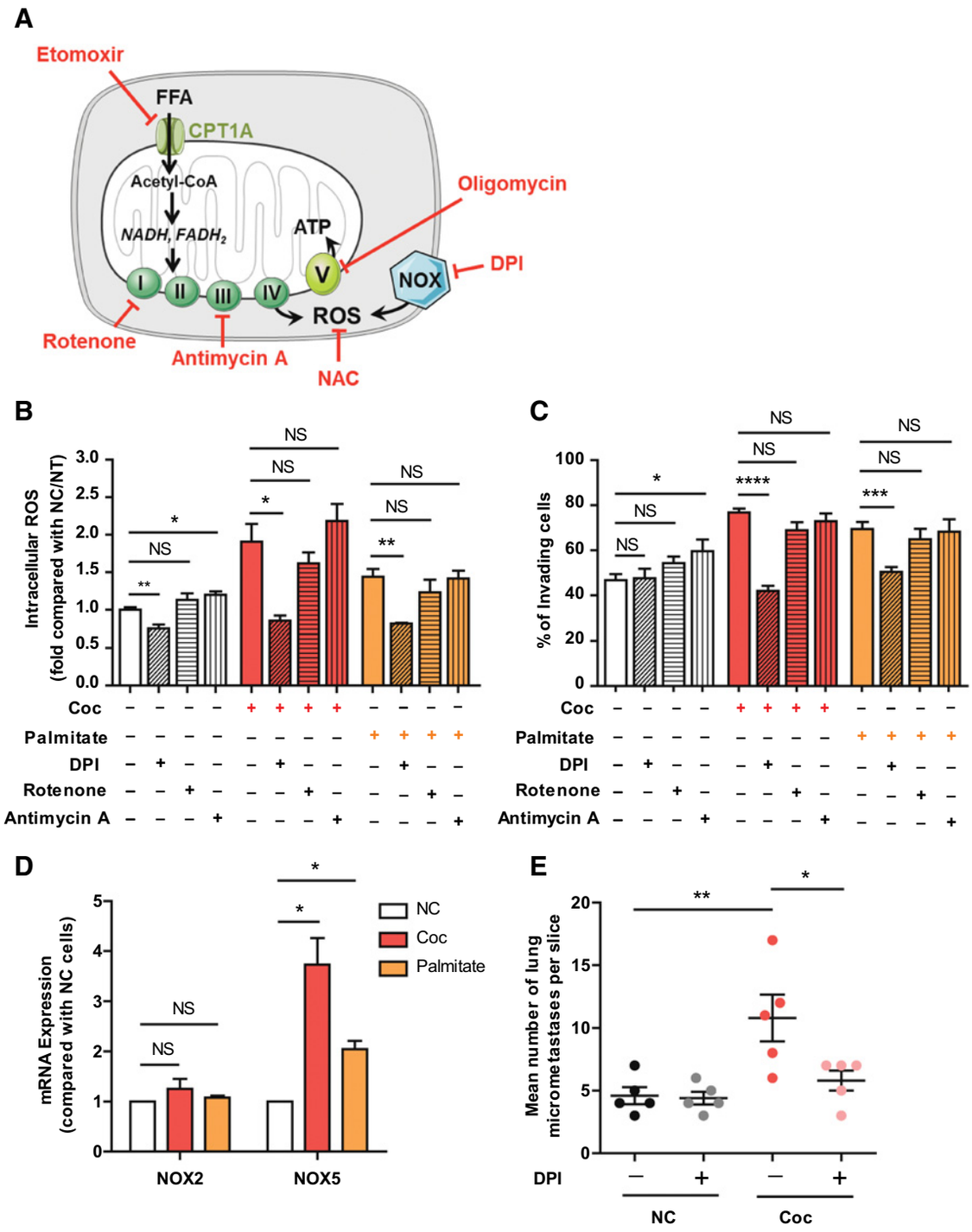

Figure 3.

FFAs stimulate tumor invasion through increased expression and activity of NOX5 in prostate cancer cells **A,** Schematic representation of the different sources of ROS and the mechanism of action of the different inhibitors used. **B,** Intracellular ROS accumulation measured by NBT assay in PC-3 cells cocultivated (Coc) or not (NC) with adipocytes or treated or not (NT) with 100 μmol/L palmitate in presence or absence of DPI (10 μmol/L), rotenone (5 μmol/L), or antimycin A (10 μmol/L). **C,** Invasion experiments toward a medium containing 10% FCS in PC-3 cells treated in similar conditions ($n = 6$). **D,** NOX2 and NOX5 mRNA expression was determined by qRT-PCR in PC-3 cells cocultivated (Coc) or not (NC) with adipocytes or treated with 100 μmol/L palmitate for 3 days. **E,** Quantification of the number of lung micrometastases in nude mice inoculated with PC-3 cells (1×10^6) cocultivated or not (NC) with adipocytes and treated (+) or not (−) with 10 μmol/L DPI for 3 days prior to intravenous injection ($n = 5$ in each group). Bars and error bars represent the means ± SEM of independent experiments ($n = 3$, unless specified otherwise). Statistically significant by Student t test (*, $P < 0.05$; **, $P < 0.01$; ***, $P < 0.001$; ****, $P < 0.0001$; NS, not significant).

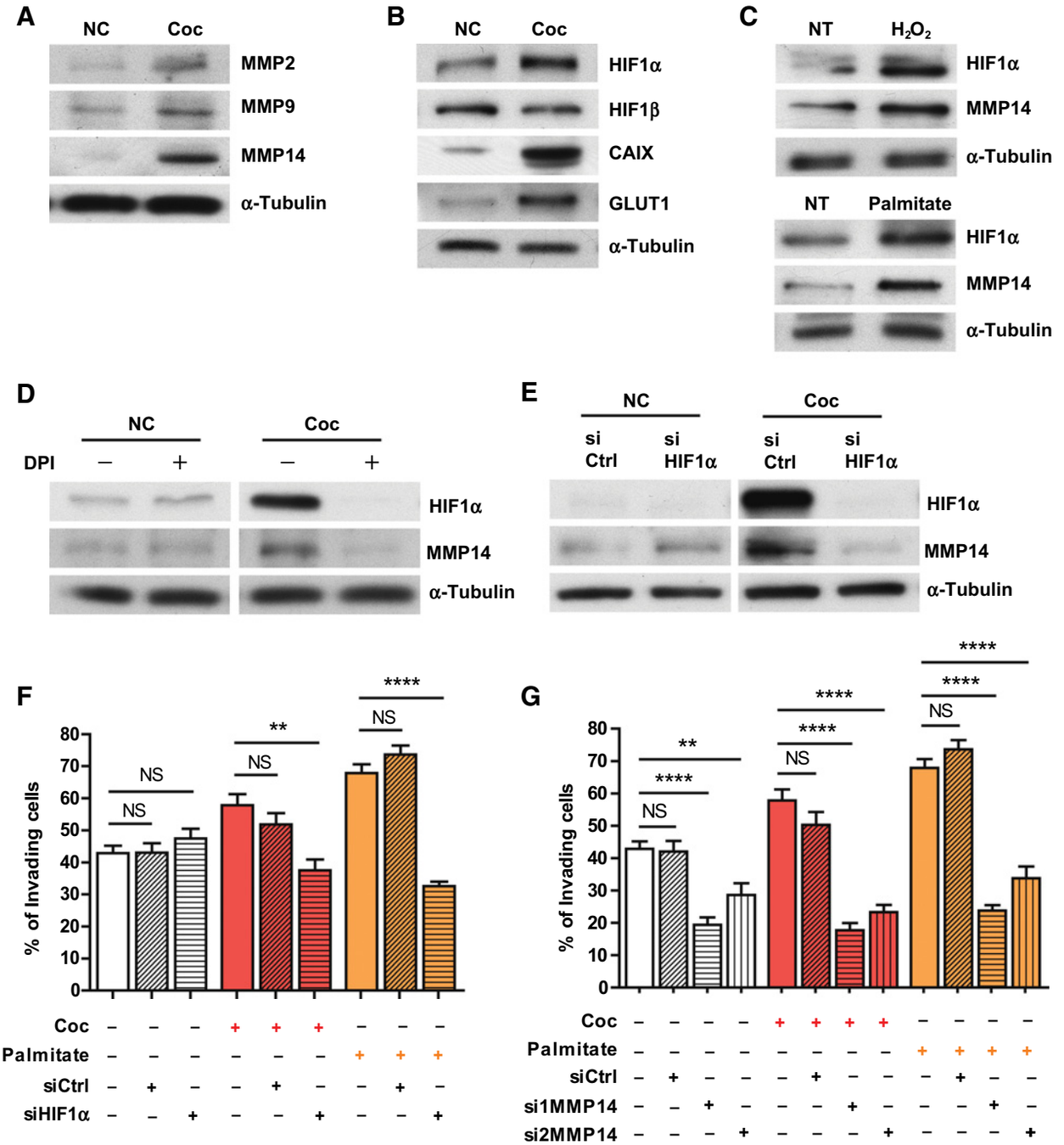

Figure 4.

The signaling cascade involved in the increase in prostate cancer invasion implicates HIF1α and MMP14 expression. **A** and **B,** PC-3 cells were cocultivated (Coc) or not (NC) with adipocytes for 3 days. **A,** Immunoblots against MMP2, MMP9, and MMP14. Note that for MMP2 and MMP9, a long exposure time (over 10 minutes) was required to reveal these blots. **B,** Immunoblots against HIF1α, HIF1β, CAIX, and GLUT1. **C,** Immunoblots against HIF1α and MMP14 in PC-3 cells treated or not (NT) with 5 μmol/L H_2O_2 or 100 μmol/L palmitate. **D,** Immunoblots against HIF1α and MMP14 in PC-3 cells cocultivated (Coc) or not (NC) with mature adipocytes for 3 days and treated (+) or not (−) with 10 μmol/L DPI. **E,** Immunoblots against HIF1α and MMP14 in PC-3 cells cocultivated (C) or not (NC) with adipocytes for 3 days and transfected with either control siRNAs (siCtrl) or directed against HIF1α (siHIF1α). **A–E,** α-tubulin is shown as a control for equal protein loading. **F,** Invasion experiments toward a medium containing 10% FCS in PC-3 cells transfected with either control siRNAs (siCtrl) or siRNAs directed against HIF1α (siHIF1α) and cocultivated (Coc) or not with adipocytes or treated with 100 μmol/L palmitate. **G,** Similar experiments were performed with PC-3 cells transfected with either control siRNAs (siCtrl) or two different siRNAs directed against MMP14 (si1MMP14 and si2MMP14). Bars and error bars represent the means ± SEM of independent experiments ($n = 4$). Statistically significant by Student t test (**, $P < 0.001$; ****, $P < 0.0001$; NS, not significant).

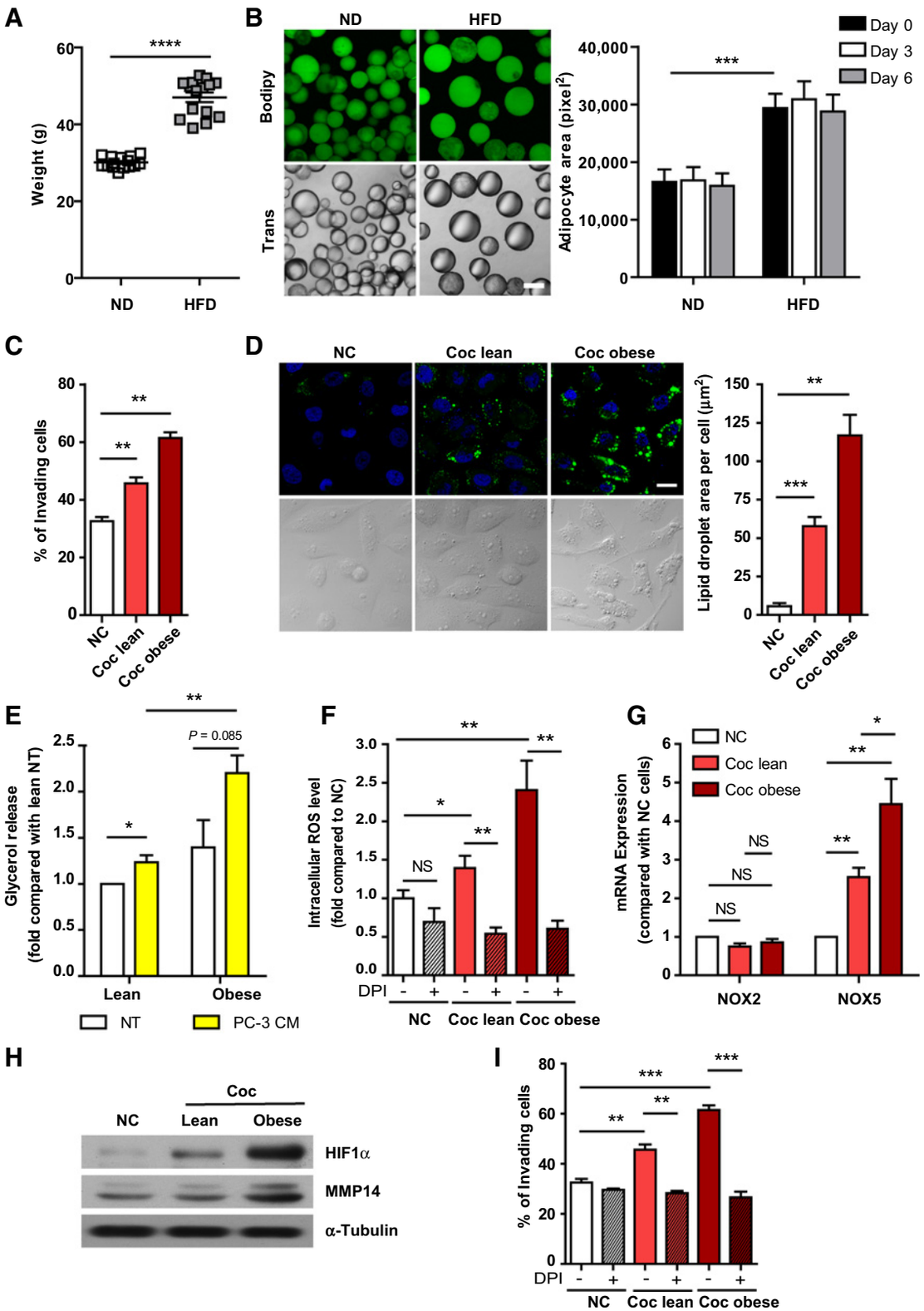

increase in lung metastases was totally reversed when PC-3 cells were treated with DPI (Fig. 3E). Taken together, our results show that coculture with adipocytes positively regulates *NOX5* that, in turn, contributes to oxidative stress and increases prostate cancer cell aggressiveness. Exogenous FFAs incorporated into prostate cancer cells can be converted into phospholipids including lysophosphatidic acids (LPA; ref. 28). LPAs have been previously shown to induce ROS generation in PC-3 prostate cancer cells in a NOX-dependent manner through activation of protein kinase C (36). Transcription of the isoform NOX5 can be increased by Ca^{2+} in a CREB-dependent manner (37) and this isoform can also be specifically activated by elevated Ca^{2+} levels through binding of Ca^{2+} to the N-terminal region (38). It has been shown previously in myocytes and pancreatic islets alpha cells that FFAs can increase cytoplasmic Ca^{2+} concentration by acting as endogenous ionophores to induce Ca^{2+} influx or by stimulating endoplasmic reticulum Ca^{2+} release (39, 40). Therefore, future studies should determine whether increased NOX5 transcription and activity are upregulated through a Ca^{2+}-dependent mechanism in response to adipocyte-derived lipids in prostate cancer cells.

A signaling pathway involving HIF1 and MMP14 increases the invasion of adipocyte-cocultivated prostate cancer cells

We next investigated the molecular events linking the increase in ROS production and cell invasion. The expression of three MMPs that have been showed to play a key role in prostate cancer progression, MMP2, MMP9, and MMP14 (also called MT1-MMP for membrane type 1 metalloprotease; ref. 41), were measured in control and cocultivated cells. As shown in Fig. 4A, MMP14 expression was strongly upregulated by coculture. Although a slight increase in MMP2 and MMP9 expression was also observed, they were far less abundant in our samples, as long exposure time was necessary to reveal their presence by Western blot analysis (Fig. 4A). To explain the link between ROS and increased MMP14 expression induced by coculture, we investigated the expression of the transcription factor HIF1 (hypoxia-inducible factor 1). HIF1 is formed by a labile α subunit (HIF1α) that is mainly targeted for normoxia-dependent degradation by the proteasomal system, whereas its β subunit, HIF1β, is constitutively expressed (42). HIF1 also responds to nonhypoxic stimuli, including ROS, which regulate HIF1α stability and transcriptional activity (42). A very recent report demonstrates that HIF1α expression is upregulated in prostate cancer cells with induced NOX5 overexpression (43). After coculture with adipocytes, HIF1α was increased when compared with control cells and, as expected, the level of the constitutively expressed subunit, HIF1β, was unchanged (Fig. 4B). The corresponding increase in HIF1 activity was shown by the increased expression of two of its target genes, the glucose transporter GLUT1 and the carbonic anhydrase IX (CAIX), a membrane spanning protein (Fig. 4B; ref. 44). Increases in MMP14 and HIF1α expression were also observed in prostate cancer cells treated with exogenous H_2O_2 or FFAs (Fig. 4C). Treatment of cocultivated cells with DPI reversed the increases in HIF1α and MMP14 induced by coculture, demonstrating the involvement of NOX in the observed effect (Fig. 4D). To directly demonstrate the role of HIF1α on the upregulation of MMP14 expression, a siRNA was used. Efficient downregulation of HIF1α expression in cocultivated cells led to a strong decrease in MMP14 expression, validating the proposed hypothesis (Fig. 4E). It is well known that MMP2 and 9 are direct target genes of HIF1 but MMP14 has been less studied, although at least one study has demonstrated the link between HIF1 and MMP14 expression in melanoma (45). The increase in cell invasion observed in cells cocultivated with adipocytes or treated with exogenous FFAs was abolished in the presence of siRNA directed against HIF1α or MMP14 (Fig. 4F and G; see Supplementary Fig. S8 for the validation of the siRNA). Taken together, our results demonstrate that coculture with adipocytes stimulates a signaling cascade involving NOX5 overexpression leading to a ROS-induced HIF1α expression that, in turn, upregulates MMP14 expression. Overexpression of HIF1α has also been described in prostate cancer cells cocultivated with bone marrow adipocytes, which are phenotypically different from classical fat depots such as PPAT (46). However, in this model, HIF1α-mediated effects persist even upon the inhibition of adipocyte-driven lipolysis, suggesting that other factors than FFAs contribute to the observed metabolic remodeling (19). Our results highlight the important role of MMP14. MMP14 is anchored to the plasma membrane by a transmembrane domain while exposing its catalytic domain on the surface of the cells and drives invasion by functioning as a pericellular collagenase (47). In prostate cancer cell lines, increased MMP14 expression has been associated with increased aggressiveness and increased transition from androgen-dependent to independent growth (41). In clinical samples, higher MMP14 mRNA levels were seen in prostate cancer compared with normal tissues (48) and its expression

Figure 5.

The deleterious crosstalk between adipocytes and tumor cells is amplified by obesity. **A,** Weight of lean (ND) and obese (HFD) mice used in the study. **B,** Left, lipid content using Bodipy staining (in green) and morphologic analysis (transmission, TRANS) of primary adipocytes embedded in a collagen I matrix, isolated from ND or HFD mice (scale bars, 100 μm; note that the images were taken on day 6 of culture). Right, quantification of the area of adipocytes embedded in a collagen I matrix, at indicated times, using ImageJ software. **C,** Invasion experiments toward a medium containing 10% FCS in PC-3 cells cocultivated (Coc) or not (NC) with adipocytes isolated from the adipose tissue (AT) of lean and obese mice. **D,** Left, PC-3 cells cocultivated (Coc) or not (NC) with adipocytes isolated from lean or obese mice were stained with Bodipy 493/503. Nuclei were labeled with DAPI. Scale bars, 20 μm. Right, quantification of lipid droplet areas performed with ImageJ software ($n = 4$). **E,** Glycerol release was measured in adipocytes isolated from lean or obese mice treated or not with PC-3 conditioned medium (PC-3 CM) for 72 hours. **F,** Intracellular ROS accumulation measured by NBT assay in PC-3 cells cocultivated (Coc) or not (NC) with adipocytes isolated from lean and obese mice and treated or not with 10 μmol/L DPI ($n = 5$). **G,** NOX2 and NOX5 mRNA expression was determined by qRT-PCR in PC-3 cells cocultivated (Coc) or not (NC) with adipocytes isolated from the adipose tissue of lean and obese mice. **H,** Expression of HIF1α and MMP14 was determined by Western blot analysis in PC-3 cells cocultivated (Coc) or not (NC) with adipocytes isolated from adipose tissue of lean and obese mice. **I,** Invasion experiments toward a medium containing 10% FCS in PC-3 cells cocultivated (Coc) or not (NC) with adipocytes isolated from the adipose tissue of lean and obese mice and treated or not with 10 μmol/L DPI. Note that the controls presented in this figure are the same as those presented in Fig. 5A as the experiments were performed simultaneously. Bars and error bars represent the means ± SEM of independent experiments ($n = 3$, unless specified otherwise). Statistical significance was determined by Student *t* test (*, $P \leq 0.05$; **, $P < 0.01$; ***, $P < 0.001$; ****, $P < 0.0001$; NS, not significant).

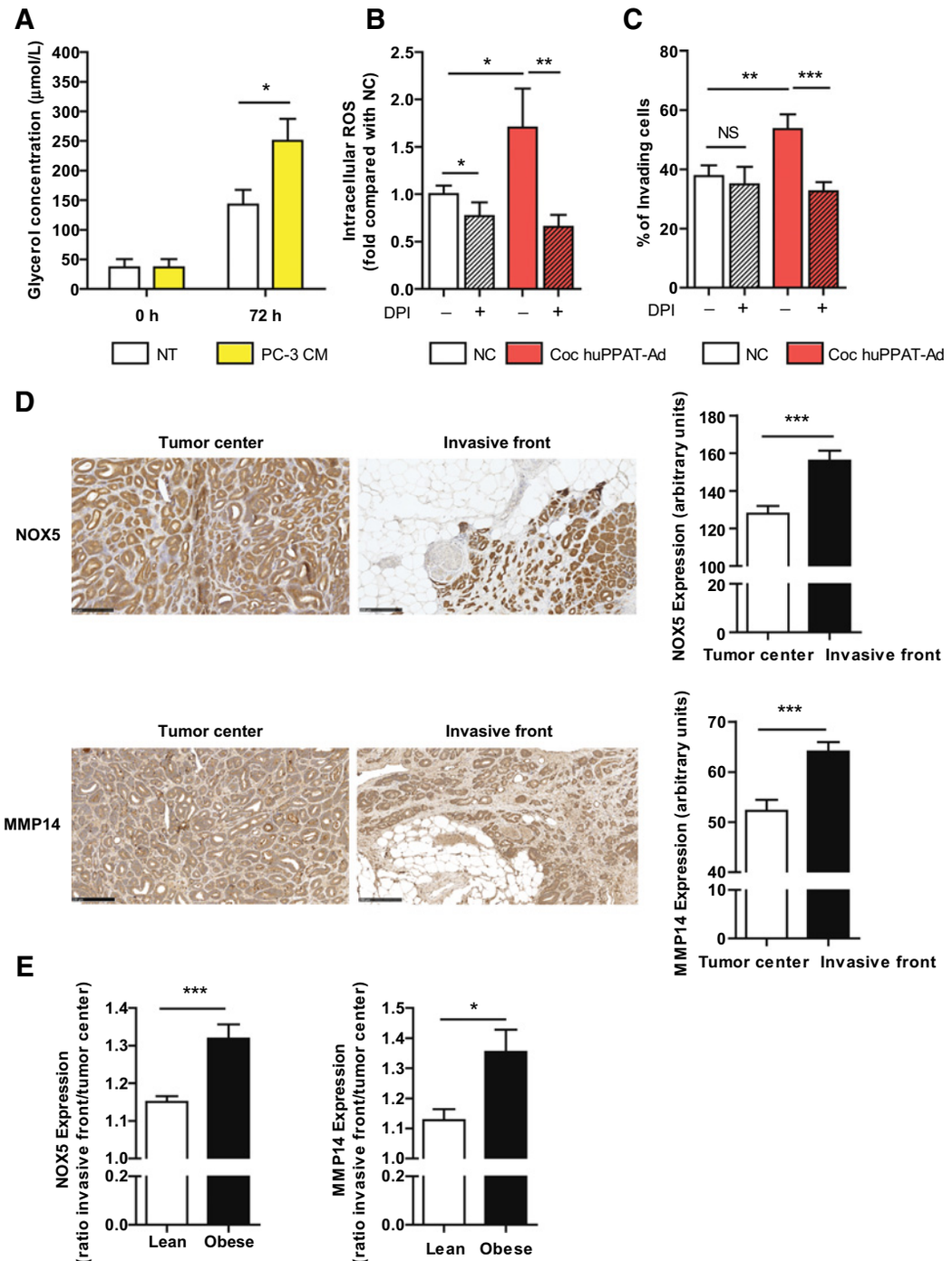

Figure 6.

The signaling pathway induced by the crosstalk between adipocytes and tumor cells exists in human tumors. **A,** Glycerol release was detected in primary adipocytes isolated from human PPAT and treated or not (NT) with PC-3 conditioned medium (PC-3 CM) for 72 hours ($n = 4$). **B,** Intracellular ROS accumulation measured by NBT assay in PC-3 cells cocultivated (Coc huPPAT-Ad) or not (NC) with adipocytes isolated from human PPAT and treated (+) or not (-) with 10 µmol/L DPI. **C,** Invasion experiments toward a medium containing 10% FCS in PC-3 cells cocultivated (Coc huPPAT-Ad) or not (NC) with adipocytes isolated from human PPAT and treated (+) or not (−) with 10 µmol/L DPI. **D,** IHC staining for NOX5 and MMP14 in human invasive prostate tumors ($n = 20$). Left, representation of a typical staining found at the tumor center or at the invasive front where tumor cells are in close contact with adipocytes (white cells). Scale bars, 250 µm. Right, quantitative expression of NOX5 and MMP14 staining using ImageJ at the tumor center and at the invasive front (mean of five independent fields per tumor). **E,** Quantitative expression of NOX5 and MMP14 staining using ImageJ in lean ($n = 10$) versus obese patients ($n = 10$). Bars and error bars represent the means ± SEM of independent experiments ($n = 3$, unless specified otherwise). Statistically significant by Student *t* test (*, $P \leq 0.05$; **, $P < 0.01$; ***, $P < 0.001$; NS, not significant).

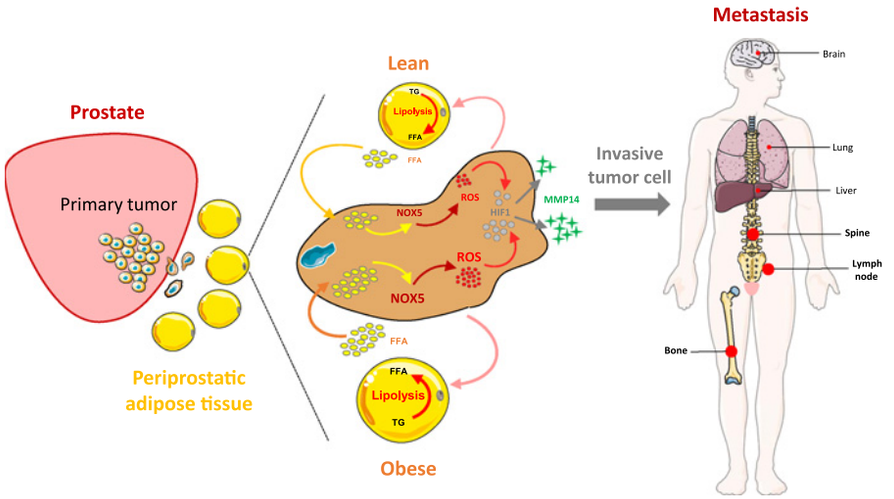

Figure 7.

Proposed model to explain the role of tumor-surrounding adipocytes in prostate cancer progression and the link with obesity. At the tumor-invasive front, a lipolytic process occurs in mature adipocytes induced by tumor secretions, which leads to the transfer and accumulation of the liberated FFAs in tumor cells. These FFAs are able to increase oxidative stress through the increased expression of one NOX isoform, NOX5. Increase in ROS levels contributes to the expression of an active form of HIF1 that, in turn, increases MMP14 expression that confers an invasive advantage to tumor cells. This signaling cascade implicating FFAs/NOX5/ROS/HIF1α/MMP14 is amplified in obesity. These tumor cells presenting increased invasive capacities could contribute to the distant dissemination of prostate cancer cells, which metastasize mainly to bone, spine, and lymph nodes.

has been associated with local dissemination (49). All these studies highlight the clinical relevance of our results (41).

Tumor aggressiveness, oxidative stress, and the depicted signaling pathway are amplified by obesity

As stated before, there is a positive association between obesity and aggressive prostate cancer, defined by an increase in local and distant dissemination (11). To investigate whether the depicted signaling pathway is amplified by obesity, prostate cancer cells were cocultivated with adipocytes isolated from the perigonadal AT of obese mice fed with either normal or high-fat diet (ND and HFD). The weight of the lean (ND) and obese (HFD) mice at the beginning of the experiments is shown in Fig. 5A. After isolation, these adipocytes were embedded in a collagen I matrix as described previously (16). As shown in Fig. 5B, these adipocytes retained their round morphology in culture for up to 6 days, with a significant and long-lasting increase in size of about 2-fold between adipocytes isolated from obese compared with lean mice. As shown in Fig. 5, the identified signaling pathway was amplified in tumor cells cocultivated with adipocytes isolated from obese animals when compared with those from lean animals. Obesity further increased *in vitro* tumor cell invasion (Fig. 5C) and tumor lipid content (Fig. 5D), a result that is explained by increased lipolysis in adipocytes from obese animals in response to tumor secretions (Fig. 5E). Accordingly, the level of ROS was significantly higher in prostate cancer cells grown in the presence of obese adipocytes (Fig. 5F) and was associated with a parallel increase in *NOX5*, but not *NOX2* (Fig. 5G), HIF1α and MMP14 protein expression (Fig. 5H). Finally, *in vitro*, the increase in prostate cancer cell invasion observed in obesity was totally abrogated by DPI treatment (Fig. 5I). In this part of our study, we demonstrate that FFAs released increased in response to tumor secretions in obesity. Obesity is associated with an increase in basal lipolysis (independent of energy deprivation) but a decrease in catecholamine-stimulated lipolysis (24). As stated above, our results demonstrate that tumor-induced lipolysis is independent of catecholamines (Supplementary Fig. S2; ref. 7), suggesting tumor cells prompt a similar mechanism of lipolysis to that in obesity. Identifying the biomolecule(s) involved in this process remains a key step to understand the adipocytes/cancer crosstalk.

Validation of the depicted signaling pathway in human tumors

We investigated whether coculture with adipocytes isolated from human PPAT reproduced the key steps of the deciphered crosstalk. In fact, it has been previously suggested that this adipose depot could present secretory and metabolic specificities (18). CM from prostate cancer cells were able to induce lipolysis in adipocytes isolated from PPAT (Fig. 6A). Coculture with adipocytes increased ROS levels in prostate cancer cells, which was abolished in the presence of DPI (Fig. 6B). Accordingly, coculture increased prostate cancer cell invasion and again this effect was abolished by DPI treatment (Fig. 6C). Unfortunately, coculture with isolated periprostatic adipocytes from obese individuals was hampered by the low percentage of obesity in the series of patients undergoing prostatectomies during the time of our study. In fact, as shown in our previous study, around 10% of the patients were obese with BMI no higher than 35 kg/m^2, a result in accordance with the incidence of obesity in Midi-Pyrénées, which is lower than the median incidence observed in France (11). To circumvent this problem, we decided to investigate the expression of two of the major actors in the depicted signaling pathway, NOX5 and MMP14, by IHC at the invasive front of human tumors, where tumor cells and adipocytes are in close contact. This strategy allowed us to include patients in a retrospective study from a more extended period. All the tumors were staged pT3a, which means that they have crossed the prostate capsule and come into contact with PPAT. In a series of 20 patients, a significant upregulation of both NOX5 and MMP14 was found at the invasive

front compared with the tumor center (Fig. 6D), which was increased by obesity (Fig. 6E). These cells, present at the invasive front, are likely to metastasize to distant sites, the bone representing the most common location of metastatic disease in prostate cancer. A bidirectional crosstalk also exists between bone marrow adipocytes and prostate cancer cells, promoting tumor progression, which appears to involve different actors such as IL1β and heme oxygenase 1 (19, 50). Again, occurrence of different mechanisms is not surprising because bone marrow adipocytes are clearly phenotypically different from classical fat depots such as PPAT (46).

In conclusion, our work unravels a new molecular pathway to explain the role of tumor-surrounding adipocytes in tumor progression, which is summarized in Fig. 7. Under tumor secretions, a lipolytic process occurs that leads to delipidation of adipocytes and to the transfer and accumulation of the released FFAs in tumor cells. In human tumors, delipidation occurs at the invasive front where cancer cells and mature adipocytes are in close contact, as we previously observed in breast tumors (3, 7). We further demonstrate that these FFAs are able to increase oxidative stress by inducing the expression of one NOX isoform, NOX5. Indeed, *NOX5* expression, as well as ROS levels, increase *in vitro* when prostate cancer cells are cocultivated with mature adipocytes obtained either from *in vitro* differentiation of the preadipocyte 3T3-F442A cell line, or primary adipocytes isolated from murine perigonadal or human periprostatic adipose tissue. Again *in vivo* overexpression of NOX5 is observed at the invasive front of human tumors. As published in the literature (31), increased oxidative stress stimulates prostate cancer invasion and the use of a NOX inhibitor completely abolished the proinvasive effect of adipocytes *in vitro* in the different coculture systems used. To explain the observed increase in tumor invasion, we demonstrated that ROS stimulate MMP14 expression through the stabilization of HIF1α. The signaling cascade, which implicates FFAs/NOX5/ROS/HIF1α/MMP14 is amplified when prostate cancer cells are cocultivated with adipocytes isolated from the adipose tissue of obese animals, and both NOX5 and MMP14 are overexpressed at the invasive front of human tumors from obese patients. Our work highlights a new molecular mechanism through which the specific adipose depot, PPAT, promotes prostate cancer aggressiveness, particularly in obesity. Specific NOX inhibitors could present a novel treatment for locally invasive prostate cancer, especially for obese patients.

Disclosure of Potential Conflicts of Interest

No potential conflicts of interest were disclosed.

Authors' Contributions

Conception and design: V. Laurent, C. Lehuédé, P. Valet, B.A. Malavaud, C. Muller

Development of methodology: V. Laurent, B.A. Malavaud

Acquisition of data (provided animals, acquired and managed patients, provided facilities, etc.): V. Laurent, A. Toulet, C. Attané, D. Milhas, S. Dauvillier, M. Cinato, S.L. Gonidec, A. Guérard, D. Garandeau, L. Nieto, B.A. Malavaud

Analysis and interpretation of data (e.g., statistical analysis, biostatistics, computational analysis): V. Laurent, A. Toulet, C. Attané, D. Milhas, A. Guérard, C. Lehuédé, L. Nieto, P. Valet, B.A. Malavaud, C. Muller

Writing, review, and/or revision of the manuscript: V. Laurent, A. Toulet, C. Attané, D. Milhas, E. Clement, A. Guérard, L. Nieto, B.A. Malavaud, C. Muller

Administrative, technical, or material support (i.e., reporting or organizing data, constructing databases): F. Zaidi, S.L. Gonidec, E. Renaud-Gabardos, B.A. Malavaud

Study supervision: B.A. Malavaud, C. Muller

Acknowledgments

The authors thank J.E. Sarry and M. Hosseini (Inserm, Cancer Research Center of Toulouse, U1037, Toulouse, France) for the use of Seahorse XFe24 analyzer. This study was supported by the French National Cancer Institute (INCA PL 2016-176 to P. Valet, B.A. Malavaud, and C. Muller), by the "Fondation Toulouse Cancer Santé" and by the Fondation ARC ("Association de Recherche contre le Cancer") Programmes labellisés 2016. Victor Laurent received a PhD fellowship from the Fondation ARC. This work also benefited from the Toulouse Réseau Imagerie (TRI)-RIO Optical Imaging Platform at Institut de Pharmacologie et Biologie Structurale (Genotoul, Toulouse, France) supported by grants from the Région Midi-Pyrénées (contrat de projets état-région), the Grand Toulouse community, the Association pour la Recherche sur le Cancer (Equipement 8505), the CNRS, and the European Union through the Fonds Européen de Développement Régional program.

The costs of publication of this article were defrayed in part by the payment of page charges. This article must therefore be hereby marked *advertisement* in accordance with 18 U.S.C. Section 1734 solely to indicate this fact.

Received July 23, 2018; revised October 2, 2018; accepted December 19, 2018; published first January 3, 2019.

References

1. Hanahan D, Weinberg RA. Hallmarks of cancer: the next generation. Cell 2011;144:646–74.
2. Duong MN, Geneste A, Fallone F, Li X, Dumontet C, Muller C. The fat and the bad: mature adipocytes, key actors in tumor progression and resistance. Oncotarget 2017;8:57622–41.
3. Dirat B, Bochet L, Dabek M, Daviaud D, Dauvillier S, Majed B, et al. Cancer-associated adipocytes exhibit an activated phenotype and contribute to breast cancer invasion. Cancer Res 2011;71:2455–65.
4. Bochet L, Lehuédé C, Dauvillier S, Wang YY, Dirat B, Laurent V, et al. Adipocyte-derived fibroblasts promote tumor progression and contribute to the desmoplastic reaction in breast cancer. Cancer Res 2013;73:5657–68.
5. Nieman KM, Kenny HA, Penicka CV, Ladanyi A, Buell-Gutbrod R, Zillhardt MR, et al. Adipocytes promote ovarian cancer metastasis and provide energy for rapid tumor growth. Nat Med 2011;17:1498–503.
6. Balaban S, Shearer RF, Lee LS, van Geldermalsen M, Schreuder M, Shtein HC, et al. Adipocyte lipolysis links obesity to breast cancer growth: adipocyte-derived fatty acids drive breast cancer cell proliferation and migration. Cancer Metab 2017;5:1.
7. Wang YY, Attané C, Milhas D, Dirat B, Dauvillier S, Guerard A, et al. Mammary adipocytes stimulate breast cancer invasion through metabolic remodeling of tumor cells. JCI Insight 2017;2:e87489.
8. Attane C, Milhas D, Hoy AJ, Muller C. Metabolic remodeling induced by adipocytes: a new Achilles' heel in invasive breast cancer? Curr Med Chem 2018:26;
9. Kapoor J, Namdarian B, Pedersen J, Hovens C, Moon D, Peters J, et al. Extraprostatic extension into periprostatic fat is a more important determinant of prostate cancer recurrence than an invasive phenotype. J Urol 2013;190:2061–6.
10. Parker AS, Thiel DD, Bergstralh E, Carlson RE, Rangel LJ, Joseph RW, et al. Obese men have more advanced and more aggressive prostate cancer at time of surgery than non-obese men after adjusting for screening PSA level and age: results from two independent nested case-control studies. Prostate Cancer Prostatic Dis 2013;16:352–6.
11. Laurent V, Guérard A, Mazerolles C, Le Gonidec S, Toulet A, Nieto L, et al. Periprostatic adipocytes act as a driving force for prostate cancer progression in obesity. Nat Commun 2016;7:10230.

12. Ribeiro R, Monteiro C, Cunha V, Oliveira MJ, Freitas M, Fraga A, et al. Human periprostatic adipose tissue promotes prostate cancer aggressiveness in vitro. J Exp Clin Cancer Res 2012;31:32.
13. Finley DS, Calvert VS, Inokuchi J, Lau A, Narula N, Petricoin EF, et al. Periprostatic adipose tissue as a modulator of prostate cancer aggressiveness. J Urol 2009;182:1621–7.
14. Lazar I, Clement E, Dauvillier S, Milhas D, Ducoux-Petit M, LeGonidec S, et al. Adipocyte exosomes promote melanoma aggressiveness through fatty acid oxidation: a novel mechanism linking obesity and cancer. Cancer Res 2016;76:4051–7.
15. Ribeiro RJ, Monteiro CPD, Cunha VF, Azevedo AS, Oliveira MJ, Monteiro R, et al. Tumor cell-educated periprostatic adipose tissue acquires an aggressive cancer-promoting secretory profile. Cell Physiol Biochem 2012;29:233–40.
16. Kaneko A, Satoh Y, Tokuda Y, Fujiyama C, Udo K, Uozumi J. Effects of adipocytes on the proliferation and differentiation of prostate cancer cells in a 3-D culture model. Int J Urol 2010;17:369–76.
17. Tokuda Y, Satoh Y, Fujiyama C, Toda S, Sugihara H, Masaki Z. Prostate cancer cell growth is modulated by adipocyte-cancer cell interaction. BJU Int 2003;91:716–20.
18. Nassar ZD, Aref AT, Miladinovic D, Mah CY, Raj GV, Hoy AJ, et al. Peri-prostatic adipose tissue: the metabolic microenvironment of prostate cancer. BJU Int 2018;121:9–21.
19. Diedrich JD, Rajagurubandara E, Herroon MK, Mahapatra G, Hüttemann M, Podgorski I. Bone marrow adipocytes promote the Warburg phenotype in metastatic prostate tumors via HIF-1α activation. Oncotarget 2016;7:64854–77.
20. Gazi E, Gardner P, Lockyer NP, Hart CA, Brown MD, Clarke NW. Direct evidence of lipid translocation between adipocytes and prostate cancer cells with imaging FTIR microspectroscopy. J Lipid Res 2007;48:1846–56.
21. Meulle A, Salles B, Daviaud D, Valet P, Muller C. Positive regulation of DNA double strand break repair activity during differentiation of long life span cells: the example of adipogenesis. PLoS One 2008;3:e3345.
22. Monferran S, Paupert J, Dauvillier S, Salles B, Muller C. The membrane form of the DNA repair protein Ku interacts at the cell surface with metalloproteinase 9. EMBO J 2004;23:3758–68.
23. Muller C, Monferran S, Gamp AC, Calsou P, Salles B. Inhibition of Ku heterodimer DNA end binding activity during granulocytic differentiation of human promyelocytic cell lines. Oncogene 2001;20:4373–82.
24. Lafontan M, Langin D. Lipolysis and lipid mobilization in human adipose tissue. Prog Lipid Res 2009;48:275–97.
25. Chirumbolo S, Bjørklund G. Can Wnt5a and Wnt non-canonical pathways really mediate adipocyte de-differentiation in a tumour microenvironment? Eur J Cancer 2016;64:96–100.
26. Braun K, Oeckl J, Westermeier J, Li Y, Klingenspor M. Non-adrenergic control of lipolysis and thermogenesis in adipose tissues. J Exp Biol 2018;221:pii: jeb165381.
27. Wu X, Daniels G, Lee P, Monaco ME. Lipid metabolism in prostate cancer. Am J Clin Exp Urol 2014;2:111–20.
28. Louie SM, Roberts LS, Mulvihill MM, Luo K, Nomura DK. Cancer cells incorporate and remodel exogenous palmitate into structural and oncogenic signaling lipids. Biochim Biophys Acta 2013;1831:1566–72.
29. Huang J, Duran A, Reina-Campos M, Valencia T, Castilla EA, Müller TD, et al. Adipocyte p62/SQSTM1 suppresses tumorigenesis through opposite regulations of metabolism in adipose tissue and tumor. Cancer Cell 2018;33:770–84.
30. Roumeguère T, Sfeir J, El Rassy E, Albisinni S, Van Antwerpen P, Boudjeltia KZ, et al. Oxidative stress and prostatic diseases. Mol Clin Oncol 2017;7:723–8.
31. Kumar B, Koul S, Khandrika L, Meacham RB, Koul HK. Oxidative stress is inherent in prostate cancer cells and is required for aggressive phenotype. Cancer Res 2008;68:1777–85.
32. Brocato J, Chervona Y, Costa M. Molecular responses to hypoxia-inducible factor 1α and beyond. Mol Pharmacol 2014;85:651–7.
33. Bedard K, Krause KH. The NOX family of ROS-generating NADPH oxidases: physiology and pathophysiology. Physiol Rev 2007;87:245–313.
34. Brar SS, Corbin Z, Kennedy TP, Hemendinger R, Thornton L, Bommarius B, et al. NOX5 NAD(P)H oxidase regulates growth and apoptosis in DU 145 prostate cancer cells. Am J Physiol Cell Physiol 2003;285:C353–69.
35. Höll M, Koziel R, Schäfer G, Pircher H, Pauck A, Hermann M, et al. ROS signaling by NADPH oxidase 5 modulates the proliferation and survival of prostate carcinoma cells. Mol Carcinog 2016;55:27–39.
36. Lin CC, Lin CE, Lin YC, Ju TK, Huang YL, Lee MS, et al. Lysophosphatidic acid induces reactive oxygen species generation by activating protein kinase C in PC-3 human prostate cancer cells. Biochem Biophys Res Commun 2013;440:564–9.
37. Fu X, Beer DG, Behar J, Wands J, Lambeth D, Cao W. cAMP-response element-binding protein mediates acid-induced NADPH oxidase NOX5-S expression in Barrett esophageal adenocarcinoma cells. J Biol Chem 2006;281:20368–82.
38. Bánfi B, Tirone F, Durussel I, Knisz J, Moskwa P, Molnár GZ, et al. Mechanism of Ca2+ activation of the NADPH oxidase 5 (NOX5). J Biol Chem 2004;279:18583–91.
39. Fang KM, Lee AS, Su MJ, Lin CL, Chien CL, Wu ML. Free fatty acids act as endogenous ionophores, resulting in Na+ and Ca2+ influx and myocyte apoptosis. Cardiovasc Res 2008;78:533–45.
40. Fujiwara K, Maekawa F, Dezaki K, Nakata M, Yashiro T, Yada T. Oleic acid glucose-independently stimulates glucagon secretion by increasing cytoplasmic Ca2+ via endoplasmic reticulum Ca2+ release and Ca2+ influx in the rat islet alpha-cells. Endocrinology 2007;148:2496–504.
41. Gong Y, Chippada-Venkata UD, Oh WK. Roles of matrix metalloproteinases and their natural inhibitors in prostate cancer progression. Cancers 2014;6:1298–327.
42. Movafagh S, Crook S, Vo K. Regulation of hypoxia-inducible factor-1a by reactive oxygen species: new developments in an old debate. J Cell Biochem 2015;116:696–703.
43. Antony S, Jiang G, Wu Y, Meitzler JL, Makhlouf HR, Haines DC, et al. NADPH oxidase 5 (NOX5)-induced reactive oxygen signaling modulates normoxic HIF-1α and p27Kip1 expression in malignant melanoma and other human tumors. Mol Carcinog 2017;56:2643–62.
44. Pouysségur J, Mechta-Grigoriou F. Redox regulation of the hypoxia-inducible factor. Biol Chem 2006;387:1337–46.
45. Hanna SC, Krishnan B, Bailey ST, Moschos SJ, Kuan PF, Shimamura T, et al. HIF1α and HIF2α independently activate SRC to promote melanoma metastases. J Clin Invest 2013;123:2078–93.
46. Horowitz MC, Berry R, Holtrup B, Sebo Z, Nelson T, Fretz JA, et al. Bone marrow adipocytes. Adipocyte 2017;6:193–204.
47. Li XY, Ota I, Yana I, Sabeh F, Weiss SJ. Molecular dissection of the structural machinery underlying the tissue-invasive activity of membrane type-1 matrix metalloproteinase. Mol Biol Cell 2008;19:3221–33.
48. Cardillo MR, Di Silverio F, Gentile V. Quantitative immunohistochemical and in situ hybridization analysis of metalloproteinases in prostate cancer. Anticancer Res 2006;26:973–82.
49. Trudel D, Fradet Y, Meyer F, Harel F, Têtu B. Membrane-type-1 matrix metalloproteinase, matrix metalloproteinase 2, and tissue inhibitor of matrix proteinase 2 in prostate cancer: identification of patients with poor prognosis by immunohistochemistry. Hum Pathol 2008;39:731–9.
50. Herroon MK, Rajagurubandara E, Diedrich JD, Heath EI, Podgorski I. Adipocyte-activated oxidative and ER stress pathways promote tumor survival in bone via upregulation of Heme Oxygenase 1 and Survivin. Sci Rep 2018;8:40.